ELSEVIER

Earth and Planetary Science Letters 133 (1995) 185–198

EPSL

The fate of slabs inferred from seismic tomography and 130 million years of subduction

Lianxing Wen, Don L. Anderson

Seismological Laboratory, 252-21, California Institute of Technology, Pasadena, CA, USA

Received 1 November 1994; accepted 26 March 1995

Abstract

The volume and location of subducted plate, since 130 Ma, are reconstructed from magnetic anomalies and updated finite rotation parameters describing relative motions in the ocean basins and between plates and hotspots. The area of subducted plate is calculated from the relative motions between overriding and overridden plates along the length of convergence in the hotspot reference frame in 5 Ma intervals. Ridge locations are reconstructed by rotating magnetic anomalies from their present to their former positions. The distances between trenches and ridges, at a certain point of time, in the spreading direction are thus estimated and are used to determine the ages of trenches, according to the spreading history recorded in present-day oceans. The thickness of the oceanic plate is obtained from the age based on the half-space cooling model. About 3.45×10^{10} km^3 of oceanic plate has been subducted during the past 130 Ma, with maximum accumulation beneath Southeast Eurasia. At spherical harmonic degree $l = 2$, where subduction flux peaks, excellent correlation is found between four seismic tomographic models at the top of the lower mantle (about 800–1100 km deep) and predicted slab locations. For some seismic models excellent correlation is also found at other degrees in that depth range. Some models also have good correlations with predicted slab locations in the deep mantle at $l = 2$. Direct comparison between subduction and seismic tomographic patterns at 800–1100 km shows that subduction history correlates with tomography very well in terms of location and amplitude of anomalies. Cold downwellings, which may be related to slabs, appear to be trapped in the mesosphere, or middle mantle. Correlations between seismic tomography and subduction over different time periods support this conclusion. There are also some correlations in the upper mantle and in the deep lower mantle, although they are generally not as significant as those in the 800–1100 km depth range. There may be a significant boundary in the mantle near the 800–1100 km depth. From a geodynamic and chemical point of view, the lower mantle may start at a depth closer to 1000 km than to 670 km.

1. Introduction

The fate of subducted slabs is controversial and the issue of whether subducting slabs penetrate the 670 km discontinuity is crucial to the nature of mantle convection. Isacks and Molnar [1] interpreted the cessation of earthquake activity at about a depth of 700 km, and the compressive nature of focal mechanisms of deep earthquakes, as evidence that the resistance of slabs increased in the transition zone. Zhou and Anderson [2] showed that some slabs tend to flatten toward horizontal as they approach the base of the upper mantle. Shearer and Masters [3] also suggested that subducting slabs are deflected horizontally at the 670 km discontinuity based on tentative correlation between regional depression of the discontinuity and subduction. Some observations from travel time studies suggested that seismic

SSDI 0012-821X(95)00064-X

anomalies extend at least several hundred kilometers below the 670 km discontinuity beneath subducting slabs in some subduction zones [4–9]. Van der Hilst et al. [10] showed that slabs beneath the Japan and Izu Bonin island arcs may be deflected at the 670 km discontinuity, whereas those beneath the northern Kuril and Mariana arcs may sink into the lower mantle. Slab deflection and penetration exist at different times in convection models characterized by an endothermic phase change in a chemically homogeneous mantle [11–16]. The negative Clapeyron slope of the phase change near the 670 km depth may preclude slabs from sinking easily, and undeformed, into the lower mantle [13–16], as originally proposed [4,5].

An alternative way to approach the problem of the fate of the slab is to match the pattern of subduction and pattern of seismic tomography at various depths in the mantle. Seismic tomography is beginning to provide more realistic mapping of the Earth as more data are accumulated. Plate tectonic models make it possible to reconstruct subduction locations and the areas of subducted plates since the breakup of Pangea. Scrivner and Anderson [17] determined regions of subduction since the breakup of Pangea at 180 Ma using paleoreconstruction maps [18]. They constructed a simple binary slab distribution function, which ignored the amount, age and subducting angle of the slabs and accounted only for the likely presence or absence of an overridden oceanic plate. They showed that the long-wavelength ($l = 2$) pattern of high-velocity anomalies (generally, cold mantle) has a correlation peak with respect to overridden oceanic lithosphere centered at transition zone depths. Correlations died off rapidly below the transition zone. Engebretson et al. [19] constructed a more detailed plate subduction history, quantifying the plate area subducted over each of the 30 Ma periods back to 180 Ma. Richards and Engebretson [20] found correlations at harmonic degree $l = 1$–3 between time-integrated subducted slab area and integrated lower mantle seismic velocities. Cadek et al [21] found good correlation between cold regions in the upper part of the lower mantle and Cenozoic subduction areas. Slab thickness and volume have been still ignored in these studies [19,20].

Subduction zones involve oceanic lithosphere with a wide range of ages. Old slabs are thicker than young slabs. In order to find the most likely depth where the slab pattern matches the seismic anomaly pattern we need more detailed reconstructions of the amount of subducted slab, which should take the age of slabs into consideration. Moreover, the detailed history of subduction can also provide constraints for convection modeling.

In this paper, we quantify slab flux further by estimating the ages and volumes of subducting plates at the various trenches. A half-space cooling model [22] is used to quantify the relation between thickness and age of the oceanic plate. We reconstruct the subducted plate area, and its average location, based on updated finite rotation poles describing the relative motions of plates, and between plates and hotspots [23,24]. We determine the age of subducted oceanic lithosphere from a digital age map of the ocean floor [25] and the finite rotation poles. We assume that the slabs accumulate at a certain depth in the mantle, beneath their average locations in each time interval. Subduction flux is evaluated by the subducted plate volume per area of the Earth surface. The actual slab distribution area is unknown, because slabs might sink into the lower mantle and may be deformed. The possible depth of slab influence is found by matching with seismic tomographic patterns. The areal distribution of the subducted plate volume flux during the past 130 Ma is compared with four seismic tomographic models at various depths throughout the mantle.

2. Detailed reconstruction of subducted slab area and thickness

An updated finite rotation model describing the relative motion of plates and between plates and hotspots is derived from the references in Table 1 [26–33]. This model is based on the assumption that the hotspots in the Atlantic and Indian Oceans are fixed relative to each other over geologically long periods of time [24]. Since the locations of old trenches are unknown, we follow Engebretson et al. [19] in assuming that trenches remain fixed relative to overriding plates during the past 130 Ma. The trenches are thus reconstructed to their former positions in the hotspot reference frame. The relative motions between overridden and overriding plate

pairs are inferred from the references given in Table 1. The finite rotations are calculated at 5 Ma intervals by assuming constant rotation during the time intervals. Stage poles and rotations are used to reconstruct the length of convergence. The length of the subduction and the area of subduction, in 5 Ma intervals, is reconstructed from the convergence history. The average positions of subduction are reconstructed by rotating the trenches, with half of the angle of rotation relative to hotspots, in each time interval. The boundaries between plates are derived directly from Müller et al. [24]. The subducted area for different time periods is shown in Fig. 1. The relative plate area subducted along these convergent boundary segments is proportional to the area of the plotted squares.

The complete history of subduction is different from Fig. 1, which only describes the subducted slab area. Different subduction zones involve oceanic lithosphere with different ages. Old slabs are thicker than slabs which involve young oceanic plate. A more accurate way to evaluate the effect of subduction is to calculate subducted slab volume. In this paper, we define the oceanic plate as mantle colder than 1100° C (i.e., the thermal boundary layer, TBL). The volume of the TBL is assumed to be the volume

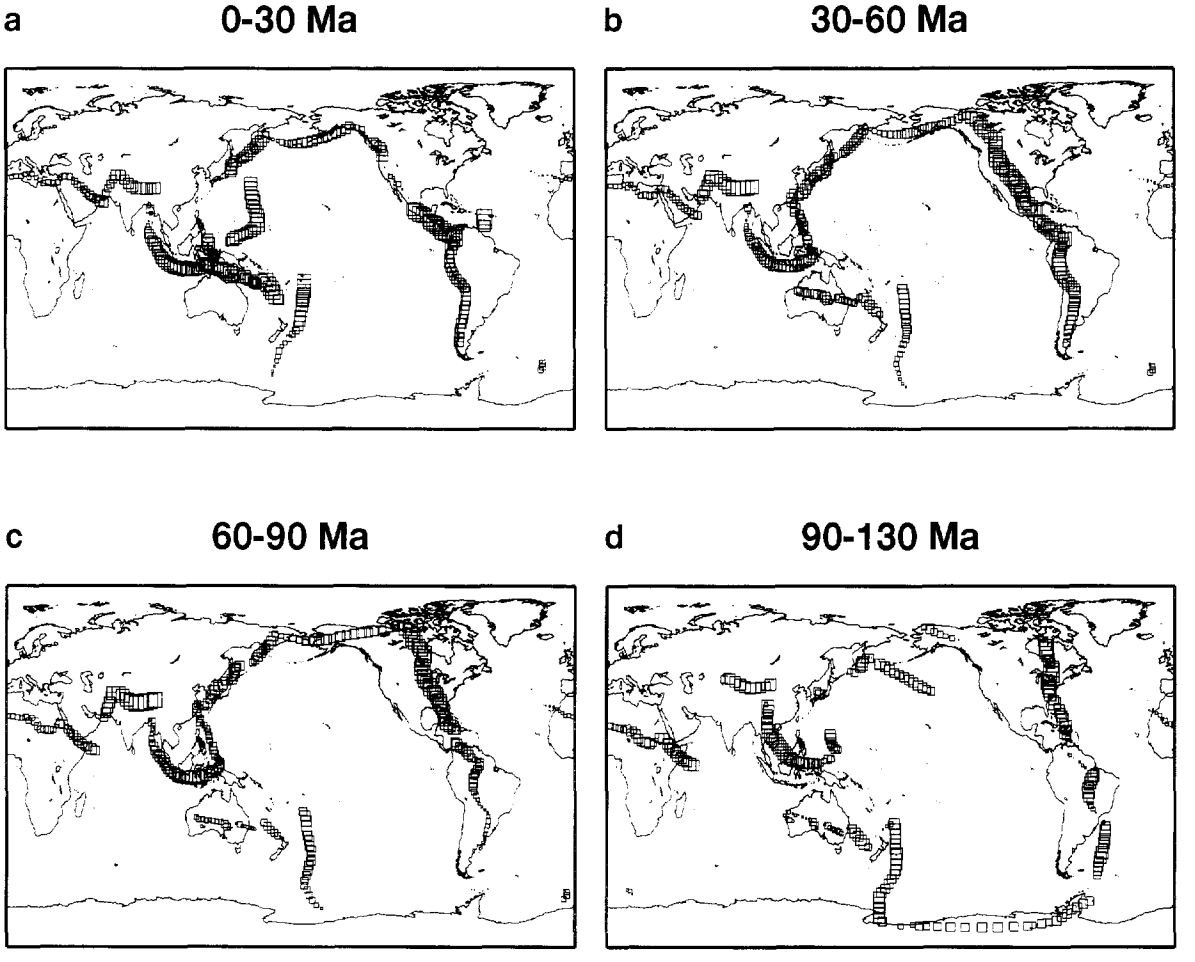

Fig. 1. The area distribution of subducted slabs during the past 130 Ma in the hotspot reference frame. The subducted area is proportional to the area of square plotted. Each plot is normalized to the maximum within that time interval. The maximum value in each plot is as follows: (a) 8.12×10^5 km^2. (b) 8.91×10^5 km^2. (c) 1.04×10^6 km^2. (d) 1.31×10^6 km^2.

of the subducted plate. Following the half-space cooling model and taking the thermal diffusivity $\kappa = 10^{-6}$ m^2 s^{-1}, one can quantify the relation between age and thickness to be $L^2 = 121 \times T$, where L is TBL thickness (km) and T is age (Ma) [25]. The age of the subducting oceanic lithosphere is determined from the distance between trenches and ridges, and using the relation between age and trench distance. Since different parts of the Pacific have different spreading histories, the Pacific Ocean is divided into four parts (north, central, southwest and southeast). A digital age grid of the ocean floor with a grid node interval of 6 arc minutes, and a self-consistent set of global isochrons and associated plate reconstruction poles, is available [25]. This allows us to measure the relation between age and distance relative to ridges in the spreading direction in those four parts of the Pacific Ocean. As an example, the average separation in the North Pacific Ocean between different aged isochrons is shown in Fig. 2. The oldest ocean floor is about 160 Ma in the Pacific. We assume the spreading rate and direction of the ridges older than 160 Ma in the Pacific are the same as those in the 140–160 Ma interval. This curve is set up as a reference spreading model for the North Pacific. The age of the oceanic lithosphere in the subduction zone is determined by the following two procedures:

(*1*) At a particular time, we take the appropriate isochron from the digital age map and rotate it to a former position using the finite rotation describing the relative motion between oceanic and overriding plate which the trench is assumed to be fixed to. This is the location of the ridge at the appropriate time (assuming that the overriding plate, i.e. trench, is fixed).

(*2*) We estimate the distance between each 20 km segment of trench and ridge in the spreading direction and find the age of the oceanic lithosphere, at the same distance from the reference isochron from the spreading history curve.

This estimated age T_0 from the spreading history curve is the age from the present day. The age determination in several subduction zones needs special treatment. One is the North American subduction zone in the last 85 Ma. Because of the presence of the Vancouver and Nazca spreading centers during the past 85 Ma [33], the oceanic lithosphere at the trenches in North America is young. Magnetic anomalies in the eastern Pacific plate have been lost beneath North America. We arbitrarily constructed a series of Vancouver–Nazca ridge locations for the past 85 Ma. The Izanagi–Pacific boundary is also

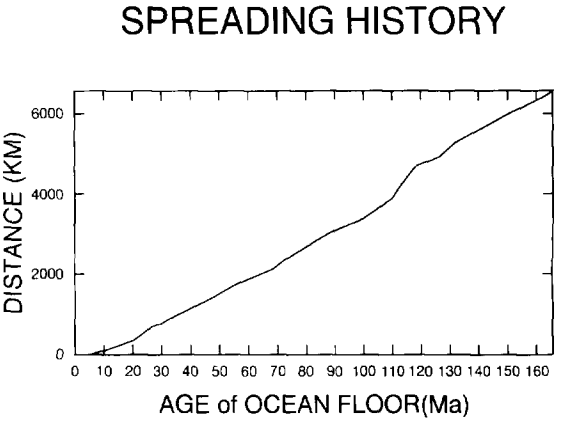

Fig. 2. The spreading history in the North Pacific based on Müller et al. [25]. The vertical axis gives the distance from isochron 5 Ma and the horizontal axis gives the age of the ocean floor.

Table 1
Sources for the reconstruction

Plate Pair	Time (Ma) From	To	Reference
NA-HS	130.0	0.0	Müller et al (1993)
SA-HS	130.0	0.0	Müller et al (1993)
EU-HS	130.0	0.0	Müller et al (1993)
AU-HS	130.0	0.0	Müller et al (1993)
AF-HS	130.0	0.0	Müller et al (1993)
AN-HS	130.0	0.0	Müller et al (1993)
IN-HS	130.0	0.0	Müller et al (1993)
AF-AR	30.0	0.0	LePichon & Gaullier (1988)
EU-NA	130.0	36.0	Srivastava & Roest (1989)
EU-NA	36.0	0.0	Lawver et al (1990)
PA-MB	130.0	90.0	Royer et al (1992)
PA-MB	90.0	49.5	Mayers et al (1990)
PA-MB	49.5	42.7	Stock & Molnar (1987)
PA-MB	42.7	0.0	Mayers et al (1990)
MB-AN	130.0	0.0	Lawver & Scotese (1987)
NZ-PA	130.0	84.0	Engebretson et al. (1984)
NZ-PA	84.0	26.0	Mayers et al. (1990)
NZ-PA	26.0	0.0	Mayers et al. (1990)
VA-PA	130.0	0.0	Royer et al (1992)
CO-PA	20.5	0.0	Royer et al (1992)
IZ-PA	130.0	84.0	Royer et al (1992)
IZ-PA	84.0	0.0	Engebretson (1984)

NA = North America; HS = hotspots; SA = South America; EU = Eurasia; AU = Australia; AF = Africa; AN = Antarctica; IN = India; PA = Pacific; MB = Marie Byrdland; NZ = Nazca; VA = Vancouver; CO = Cocos; IZ = Izanagi.

unknown, as is the behavior of the Java trench. Few magnetic anomalies are left in the Java trench today. The oceanic remnant of Tethys is about 145 Ma old (south of Indonesia, near the Java trench). The magnetic anomalies observed on the Indian Ocean floor near the Java trench are nearly symmetric with respect to the 47 Ma isochron, suggesting the cessation of spreading at that time, and indicate a spreading rate of about 5.7 cm y^{-1}. Tethys is assumed to have these characteristics. Its ridge ceased spreading at 47 Ma. The locations of the Tethys ridges are reconstructed based on these assumptions. Subduction in the Java trench, due to the spreading of Tethys before 47 Ma, is added into the calculation.

The volume of the subducted plate is reconstructed by multiplying the area and thickness of subducted slabs (TBL) in each 5 Ma interval. Fig. 3 shows the history of subducted slab volume during the past 130 Ma. About 3.45×10^{10} km^3 of oceanic plate has been subducted during this time. The subducted slab volume pattern is different from the area pattern. During the past 60 Ma subducted volume under North America is small because the slabs were very young when subducted, even though a large

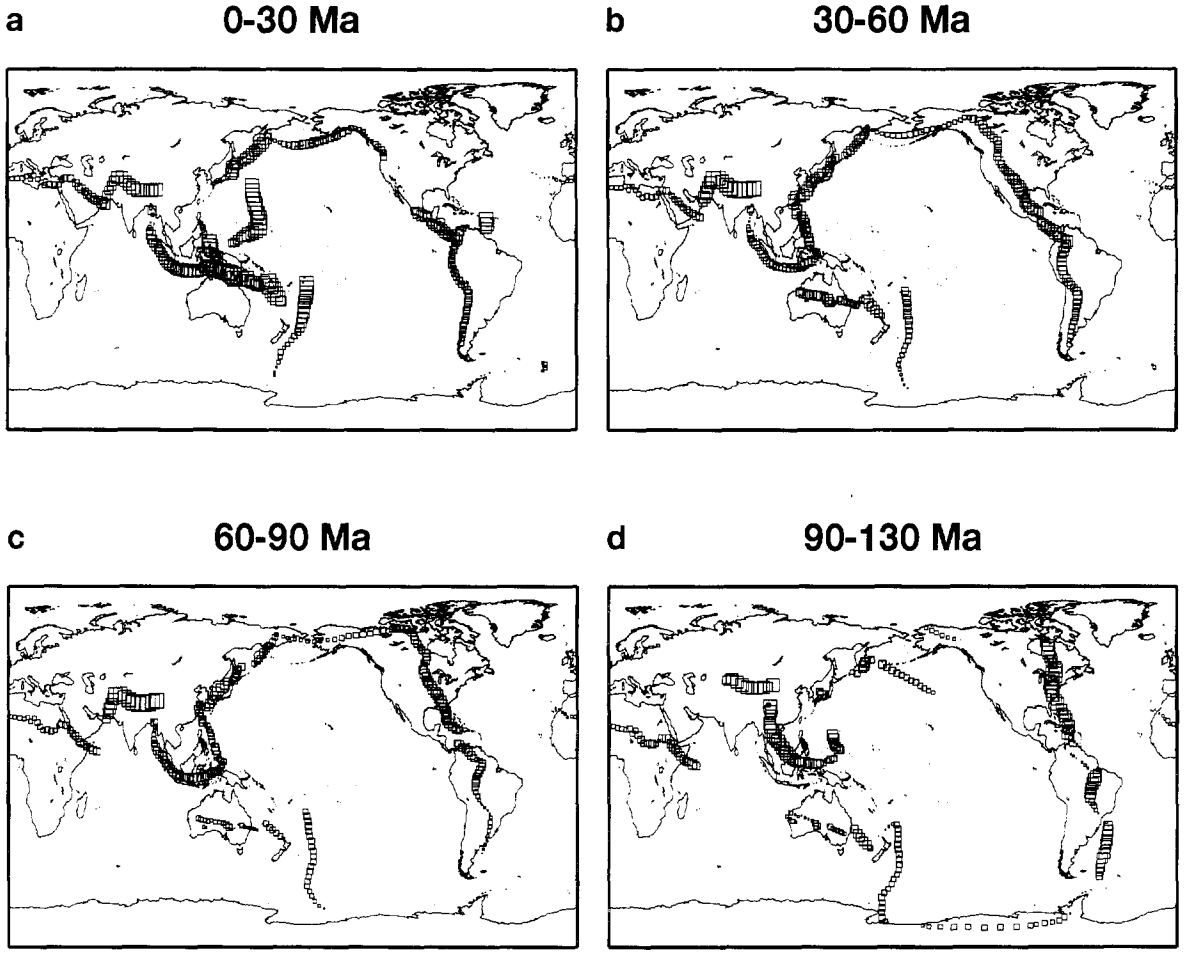

Fig. 3. Subduction history during the past 130 Ma in the hotspot reference frame. The subducted volume is proportional to the area of square plotted. Each plot is normalized to the maximum within that time interval. The maximum value in each plot is as follows: (a) 9.49×10^7 km^3. (b) 1.25×10^8 km^3. (c) 1.76×10^8 km^3. (d) 1.85×10^8 km^3.

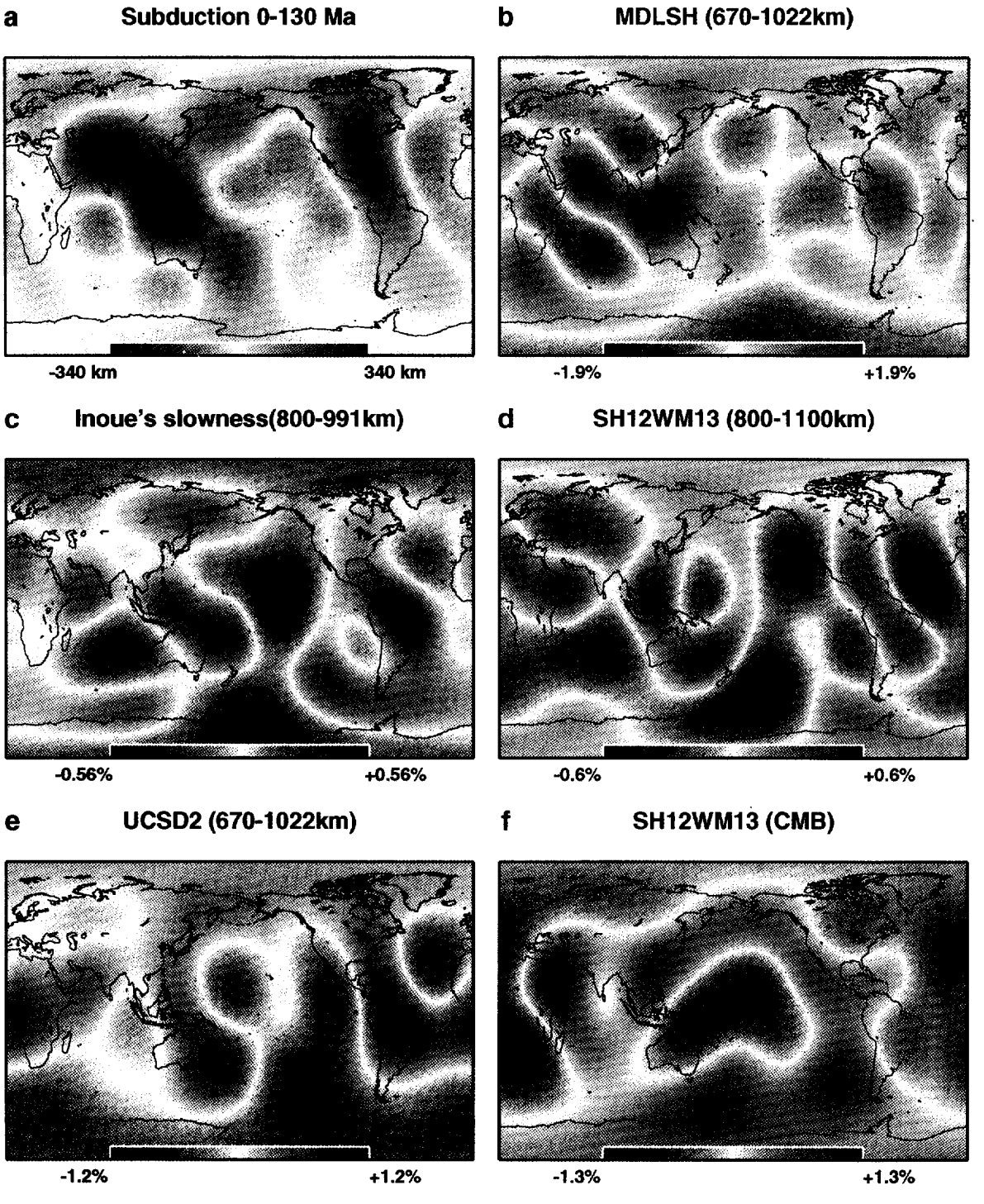
a
Subduction 0-130 Ma
-340 km
340 km
b
MDLSH (670-1022km)
-1.9%
+1.9%
c
Inoue's slowness(800-991km)
-0.56%
+0.56%
d
SH12WM13 (800-1100km)
-0.6%
+0.6%
e
UCSD2 (670-1022km)
-1.2%
+1.2%
f
SH12WM13 (CMB)
-1.3%
+1.3%

Table 2
Correlations between 0–130 Ma subduction and MDLSH

Depth, km	0-130 Ma					
	l=1	l=2	l=3	l=4	l=5	l=6
0– 220	0.56	-0.34	-0.42	0.01	0.13	0.13
220– 400	-0.51	0.42	-0.12	0.31	0.18	0.15
400– 670	-0.39	0.58	-0.03	0.40	0.27	0.14
670–1022	0.96	0.82	0.63	0.76	-0.20	0.25
1022–1284	0.38	0.16	0.17	0.51	0.22	0.20
1284–1555	-0.45	0.22	0.59	-0.48	0.30	0.09
1816–1555	0.68	0.67	0.47	-0.58	0.26	0.10
1816–2088	0.65	0.33	0.04	0.22	0.19	0.05
2088–2359	0.76	0.37	0.01	0.54	0.12	-0.20
2359–2630	0.80	0.54	0.31	0.30	0.09	-0.22
2630–2891	0.51	0.57	0.21	0.60	0.24	-0.13

Table 3
Correlations between 0–130 Ma subduction and UCSD2

Depth, km	0-130 Ma					
	l=1	l=2	l=3	l=4	l=5	l=6
20– 120	0.11	-0.29	0.36	0.48	0.29	0.31
120– 220	0.06	0.11	0.28	0.57	0.28	0.30
220– 400	0.02	0.62	0.14	0.64	0.29	0.00
400– 670	0.14	0.58	0.29	0.42	0.37	-0.49
670–1022	0.23	0.51	0.43	0.50	0.36	0.74
1022–1284	-0.70	0.89	0.48	0.39	-0.07	0.33
1284–1555	-0.98	0.95	0.61	-0.25	-0.04	-0.02
1555–1816	-0.77	0.83	0.44	-0.14	0.39	-0.48
1816–2088	-0.10	0.72	0.22	0.10	0.34	-0.48
2088–2359	0.30	0.77	0.19	0.10	0.06	-0.03
2359–2630	0.22	0.71	0.00	0.09	-0.04	-0.53
2630–2891	0.04	0.71	0.03	0.20	-0.01	-0.35

area was subducted (Fig. 2b and c). A large amount of material subducted in the 30–60 Ma and 60–90 Ma intervals between India and Eurasia because of the thick plate and the rapid movement of India toward Eurasia.

The 0–130 Ma subducted slab flux, up to spherical harmonic degree $l = 6$, is shown in the Fig. 4a. The maximum accumulation of subducted material occurs under Southeast Eurasia. There are large volumes of slab beneath the India–Eurasia boundary, Southeast Eurasia, Southeast Australia and the Americas.

3. Correlations between subducted slabs and seismic tomographic models

One way to quantitatively compare the subduction pattern with seismic velocity patterns is to calculate the correlation coefficients. We use four seismic models (MDLSH [34], SH12WM13 [35], UCSD2 (not an official name) [36] and Inoue's [37]). The seismic tomographic models are not entirely consistent with each other, because they are obtained from different datasets and use different smoothing parameters. The spherical harmonic expansion of the time-integrated subducted slabs during the past 130 Ma exhibits a maximum at $l = 2$ and $l = 1$. The correlation coefficients between slab flux and the seismic tomographic models are listed in TablesTable 2 Table 32Table 4-Table 5-5. Correlations which are significant at greater than the 90% confidence level are underlined. There are excellent correlations for most of the models (except UCSD2) over the depth range 800–1022 km (670–1022 km for MDLSH, 800–1100 km for SH12WM13, and 800–1435 km for Inoue's model) at degree $l = 1$, 2 and 4. There are also some correlations in the deep mantle. For UCSD2, excellent correlations are found over the depth interval 1022–2359 km at degree $l = 2$. Negative correlations at degree $l = 1$ for some models (UCSD2 and Inoue's model) at these depth ranges are of doubtful significance because of the low power at degree $l = 1$ for both those models. The power at degree $l = 1$ is about 50% (UCSD2 for a depth range of 1022–1284 km and Inoue's model for a depth range of 800–1435 km) of that at degree $l = 2$. Subduction also has some correlations with tomographic patterns at the core–mantle boundary (CMB).

Correlations between subduction in different time intervals and seismic models at degree $l = 2$ are listed in TablesTable 6 Table 76Table 8-Table 9-9. Subduction in the past 30 Ma correlates with the seismic models very well in most of the upper mantle and the upper part of the lower mantle. Poor

Fig. 4. Comparison of subduction patterns (a) and seismic velocity anomaly patterns at the depth range 800–1100 km (b–e) and at the CMB (f). The blue region indicates large amount of subduction in the subduction model and high velocity or low slowness anomaly in seismic tomography models. All models are truncated at spherical harmonic degree $l = 6$.

Table 4
Correlations between 0–130 Ma subduction and Inoue

Depth, km	0-130 Ma					
	l=1	l=2	l=3	l=4	l=5	l=6
0– 29	-0.03	-0.70	-0.26	0.05	0.03	-0.12
29– 78	-0.38	-0.71	-0.32	0.00	0.15	-0.08
78– 148	-0.38	-0.74	-0.34	0.07	0.23	-0.07
148– 238	0.13	-0.49	-0.30	0.04	0.19	-0.07
238– 348	0.01	-0.23	-0.42	-0.10	0.15	-0.10
348– 478	0.07	0.45	-0.16	0.13	0.20	-0.02
478– 629	-0.87	0.63	-0.36	-0.13	0.22	-0.16
629– 800	-0.46	0.57	-0.12	-0.19	0.12	-0.03
800– 991	-0.76	0.87	0.69	0.58	0.00	0.28
991–1203	-0.97	0.92	0.57	0.36	-0.30	0.21
1203–1435	-0.72	0.77	0.79	0.08	0.11	0.44
1435–1688	0.18	0.72	0.36	-0.13	-0.03	0.22
1688–1960	0.72	-0.24	0.36	-0.42	0.09	0.16
1960–2253	0.81	0.52	0.37	-0.68	0.03	-0.01
2253–2566	0.38	0.57	-0.02	-0.30	-0.24	0.08
2566–2900	0.83	0.66	0.16	-0.02	-0.57	-0.20

correlation is found below the 1555 km depth. For subduction older than 30 Ma, little correlation is found with upper mantle seismic models. The most significant correlations are found in the upper part of the lower mantle. Correlations between 90–130 Ma subduction and seismic tomography appear to occur in the upper part of the lower mantle and near the CMB. Although the correlations change for different time intervals, good correlations are most persistent in the upper part of the lower mantle (800–1500 km) (Tables 6–9). We suggest that the mantle between the 400 km discontinuity and about 1000 km be referred to as the mesosphere (for 'middle mantle').

Table 5
Correlations between 0–130 Ma subduction and SH12WM13

Depth, km	0-130 Ma					
	l=1	l=2	l=3	l=4	l=5	l=6
200– 500	-0.15	0.62	0.25	0.67	0.37	-0.02
500– 800	0.03	0.58	0.19	0.50	0.47	0.20
800–1100	0.91	0.92	0.50	0.54	0.35	0.27
1100–1400	0.48	0.61	0.45	0.22	0.19	-0.06
1400–1700	0.14	0.63	0.33	-0.34	0.06	0.03
1700–2000	0.52	0.79	0.28	-0.38	0.29	0.24
2000–2300	0.86	0.79	0.20	-0.36	0.22	0.09
2300–2600	0.78	0.70	0.08	-0.20	-0.14	-0.03
2600–2891	0.73	0.57	0.25	0.22	-0.27	-0.04

Table 6
Correlations between MDLSH and subduction at different time intervals

Depth, km	degree l=2			
	0-30 Ma	30-60 Ma	60-90 Ma	90-130 Ma
0– 220	0.11	-0.52	-0.64	-0.26
220– 400	0.85	0.12	0.02	0.45
400– 670	0.93	0.33	0.21	0.59
670–1022	0.94	0.67	0.55	0.80
1022–1284	-0.23	0.26	0.25	0.28
1284–1555	0.14	0.22	0.14	0.28
1555–1816	0.34	0.68	0.74	0.69
1816–2088	-0.17	0.48	0.57	0.36
2088–2359	0.07	0.40	0.39	0.45
2359–2630	0.17	0.56	0.58	0.64
2630–2891	0.19	0.60	0.62	0.66

4. Interpretations

Correlations give no information about cause and effect, but one interpretation of the good correlations is that subduction in the past 130 Ma had a much greater effect on the seismic anomalies in the upper part of the lower mantle (depth of about 800–1100 km) than elsewhere. Slab penetration into the lower mantle or mesosphere may be one explanation.

It is useful to compare the subduction map pattern with seismic velocity patterns at various depths in the mantle. Subduction pattern and seismic anomaly patterns at a depth range of 800–1100 km are shown in Figs. 4a–e. Subduction correlates well with seismic anomalies in terms of location and relative amplitude at this depth range. Large subduction vol-

Table 7
Correlations between SH12WM13 and subduction at different time intervals

Depth, km	degree l=2			
	0-30 Ma	30-60 Ma	60-90 Ma	90-130 Ma
200– 500	0.77	0.42	0.36	0.66
500– 800	0.93	0.34	0.21	0.58
800–1100	0.89	0.82	0.74	0.90
1100–1400	0.26	0.77	0.78	0.48
1400–1700	0.03	0.82	0.88	0.59
1700–2000	0.33	0.85	0.87	0.84
2000–2300	0.38	0.81	0.82	0.86
2300–2600	0.23	0.75	0.78	0.77
2600–2891	0.00	0.72	0.78	0.60

umes beneath Southeast Eurasia, the India–Eurasia boundary, the East Australian plate and North and South America correlate with high velocity anomalies beneath those regions. The absence of subduction, or small subduction volumes, correlates with slow or normal seismic velocities. Anomaly patterns at the CMB for various tomographic models are shown in FigsFig. 5. 4f and 5a–c. Although there are some individual correlations, the large-scale patterns no longer agree with the subduction pattern. One explanation is that slabs might be trapped in the depth interval 800–1100 km, or, considering the resolution, near 900 or 1000 km. Similar results were obtained by Ray and Anderson [40] and Cadek et al [21].

Correlations between tomographic models and subduction over different time intervals may reveal more information about the effects and fate of the subducted slabs. Recent subduction (0–30 Ma) correlates with seismic tomographic models in most of the upper mantle and the upper part of the lower mantle. Note the good correlations at depths of 800–1100 km for recent subduction. Excellent correlations in the mesosphere at $l = 2$, for subduction in other time intervals, support the hypothesis that cold downwellings might be trapped in this depth region for a period of time. We need to stress again, however, that correlations alone cannot establish cause and effect.

Table 8
Correlations between Inoue's slowness and subduction at different time intervals

	degree l=2			
Depth, km	0-30 Ma	30-60 Ma	60-90 Ma	90-130 Ma
0- 29	-0.43	-0.79	-0.76	-0.61
29- 78	-0.43	-0.80	-0.77	-0.62
78- 148	-0.49	-0.82	-0.79	-0.62
148- 238	-0.35	-0.60	-0.57	-0.32
238- 348	-0.23	-0.32	-0.31	-0.06
348- 478	0.40	0.29	0.23	0.61
478- 629	0.78	0.43	0.31	0.70
629- 800	0.77	0.36	0.26	0.63
800- 991	0.91	0.75	0.67	0.82
991-1203	0.51	0.98	0.98	0.88
1203-1435	0.34	0.80	0.82	0.81
1435-1688	0.25	0.85	0.90	0.68
1688-1960	-0.74	0.00	0.09	-0.19
1960-2253	-0.06	0.69	0.78	0.50
2253-2566	0.06	0.66	0.70	0.63
2566-2900	0.17	0.74	0.77	0.70

Table 9
Correlations between UCSD2 and subduction at different time intervals

	degree l=2			
Depth, km	0-30 Ma	30-60 Ma	60-90 Ma	90-130 Ma
20- 120	0.11	-0.53	-0.56	-0.16
120- 220	0.43	-0.16	-0.19	0.22
220- 400	0.71	0.46	0.40	0.63
400- 670	0.88	0.37	0.23	0.57
670-1022	0.86	0.29	0.16	0.51
1022-1284	0.77	0.85	0.77	0.85
1284-1555	0.80	0.91	0.85	0.90
1555-1816	0.42	0.90	0.93	0.79
1816-2088	0.23	0.82	0.87	0.72
2088-2359	0.36	0.80	0.82	0.82
2359-2630	0.24	0.76	0.77	0.78
2630-2891	0.24	0.76	0.77	0.78

The 670 km discontinuity is not the only possible mechanical boundary in the deep mantle. Kawakatsu and Niu [39] have recently reviewed evidence for a sharp mantle discontinuity in the depth interval 900–1000 km. This appears to be a global feature and may mark a chemical change or change in intrinsic density. If this discontinuity is a phase change boundary, it would probably vary little in depth. A large depth variation would make it more difficult to detect. The mantle may also have relatively high viscosity below this depth. Ray and Anderson [40] found statistically significant correlations between high velocities in the depth range 220–1022 km and integrated slab locations, and between low velocities and slab locations at the 1022–1284 km depth. There may, therefore, be a buoyancy or rheological barrier near the depth of 1000 km in the mantle. Slabs might be trapped at this depth, either permanently or for a period of time.

Slab migration in the hotspot reference frame is generally retrograde (Figs. 1 and 3) (i.e., the migration direction is opposite to the subduction direction) [41,42]. The seismic patterns at the CMB will correlate with 'future' subduction if subduction migration remains retrograde (Figs. 4f and 5a–c). An interpretation is that downwellings in the lower mantle may

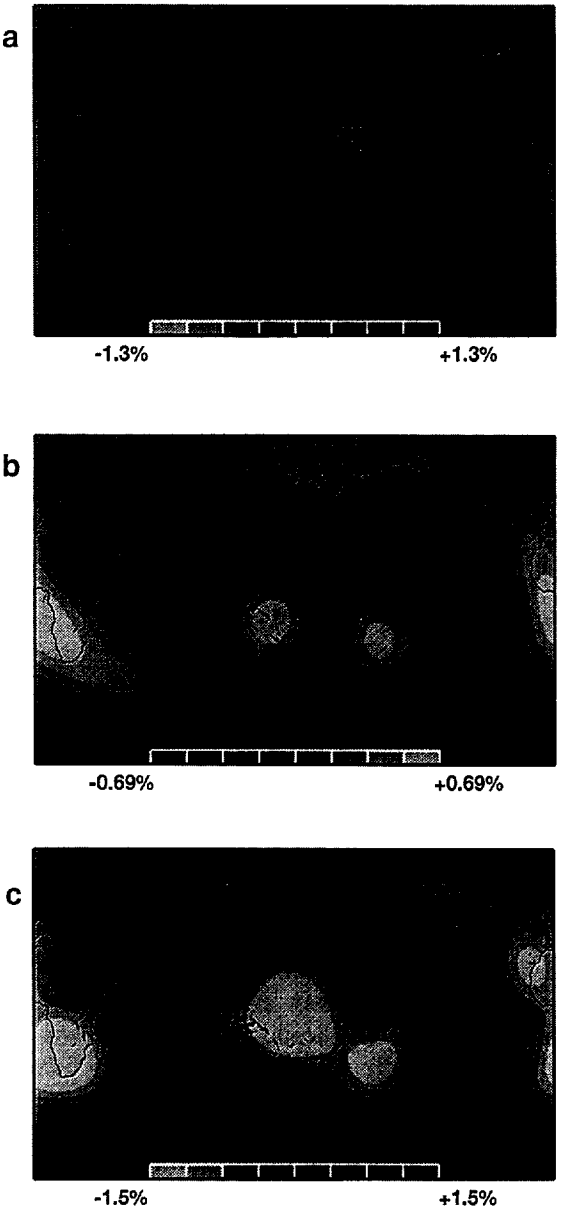

Fig. 5. Seismic anomalies at the CMB for various tomographic models: (a) MDLSH. (b) Inoue's slowness. (c) UCSD2. All models are truncated at spherical harmonic degree $l = 6$.

control where continents accumulate and where subduction takes place. Seismic anomalies in the lower mantle, beneath subduction zones, may be the result of downwellings in the lower mantle rather than slab penetration. Even if the mantle is chemically layered there will be a feedback between upper and lower layer convection and between subduction locations and downwellings in the system. A previous subduction regime may control locations of cold downwellings in the deep mantle [43].

The differing results for the different seismic models indicate that, perhaps, none of the models is an adequate representation of the Earth, even at long wavelengths. It is therefore useful to look also at high correlation coefficients, even if they are not highly significant. The highest correlations are generally in the transition region and the top of the lower mantle, as conventionally defined. The mantle above the 400 km depth generally has much lower correlation coefficients, except sometimes at $l = 4$, or at $l = 2$ for certain 30 Ma intervals. This poor correlation may be due to the dominant role of cratonic mantle at shallow depths. Several models have good correlation at $l = 2$ for parts of the deep lower mantle (1000–1600 km) for older subduction zones (30–130 Ma), but generally not for $l \neq 2$. This may suggest that the high velocities, in the deep mantle, associated with past subduction zones may represent a pre-existing condition [43] rather than be the result of relatively narrow slabs [4,5] or episodic flushing events [13,14,16]. If the lower mantle has high viscosity, its convection pattern may be much more stable, and long-lived, than upper mantle convection, and it may modulate the pattern of convection in the upper mantle.

5. Discussion

One must be cautious when interpreting correlations between geophysical fields. We assume that high-velocity anomalies (HVA) represent cold mantle. Cold material is generally dense, so cold high-velocity regions may represent cold downwellings. Of course, cold downwellings will slow or stop if a buoyancy, viscosity or phase change barrier is encountered [44].

It is difficult to disentangle cause and effect. HVAs may be the signature of slabs subducted from the surface. Or, the locations of subduction zones may be controlled by pre-existing cold downwellings

[43]. Even bottomed-out slabs can cause cold downwellings, or the absence of upwellings, in the overlying mantle. They can also, with possibly a considerable time delay, cause downwellings in the underlying mantle. Continents may periodically collect over cold downwelling mantle, forcing their associated subduction zones to occur over pre-existing HVAs.

Excellent correlations in the upper part of the lower mantle could also be the result of downwellings of the lower mantle, triggered by the cooling of slab accumulated at the 670 km discontinuity. However, if this is the case, good correlations at transition zone depths (400–670 km) might also be expected, because the cold slabs should also cool the bottom of the upper mantle. For some seismic models there is little correlation between subduction flux and seismic anomalies in the upper mantle and between 670 and 800 km. Correlations in the upper mantle and transition region are generally good only for recent subduction (0–30 Ma) or for degree $l = 4$.

The 670 km discontinuity is generally believed to result primarily from the phase change γ-spinel $\rightarrow$ perovskite + magnesiowüstite, which has a negative Clapeyron slope. If the slab is identical in composition to the lower mantle, the former will still be in the low-density phase when it encounters the discontinuity. The slab can only penetrate the boundary when sufficient negative thermal buoyancy has accumulated [14–16]. If the slab has a different composition from the lower mantle, or if trench migration precludes slab pile-up, it may not be able to penetrate at all. For example, a garnet-rich slab can be less dense than the lower mantle over a considerable depth range [44]. However, the interaction of a cold slab with the 670 km discontinuity is probably complex and variable [45–47]. The cold interior of a slab may incompletely transform to a high-pressure phase [48]. Kinetic effects may also slow the transitions in the slab.

The situation is complicated somewhat by the low radial resolution of the tomographic models and relatively small effect of temperature on density and seismic velocity in the lower mantle. It is even not clear if cold slabs would show up in $l = 2$ expansions of seismic velocity, and why they should not show up at other wavelengths.

Things become more complicated by the possible intervention of non-thermal controls on density and seismic velocity. The slab is cold but it may differ in its chemistry and phase relations from the surrounding mantle. If the interior of the slab, at transition zone depths, is eclogitic (garnet + clinopyroxene or majorite), or metastable olivine, it may have intrinsically lower velocity and density than the surrounding mantle [46,49]. The low temperature would increase velocity and density. The seismic velocity in a cold dense slab lying on a chemical boundary under isostatic equilibrium could be faster than that of the mantle above the discontinuity but slower than that on the other side. Seismic waves would see the average difference. Also, the cold interior of the slab may be a different, perhaps metastable, phase assemblage from the warm exterior [48]. Colder than average mantle above 400 km or below 900 km is probably fast and dense but the situation is more ambiguous in the vicinity of phase changes or mantle discontinuities, or where kinetics may play a role.

It should also be kept in mind that the depths of velocity anomalies in global tomographic studies are uncertain by about 200 km. For example, the excellent correlation at 670–1022 km for MDLSH can be explained either by slab deflection at 670 km or penetration into the lower mantle. Results from the various correlations do not exclude the possibility of slab deflection at 670 km for some slabs.

Anderson [46,50] showed that the subducting oceanic crust is less dense than the lower mantle, at least to depths of 750 km. This is largely due to the wide stability field of garnet [49]. The endothermic nature of most phase changes near 670 km makes it difficult for slabs to penetrate the boundary unless they are very cold or unless pushed through by the accumulated weight of the overlying slab (avalanching). The top of the lower mantle has a high gradient in elastic properties and is deleted in equation of state fits. It is not part of the discussion regarding composition of the lower mantle or chemical homogeneity, or otherwise, of the mantle. It is, however, that part of the lower mantle for which some evidence exists for slab penetration "into the lower mantle" [51]. Slab penetration to about 900 km does not preclude an intrinsically high density, due to chemical differences, for most of the lower mantle.

There are several ways to interpret the correlations between subduction and seismic anomalies. Most investigators focus on the role played by the

670 km discontinuity. Does subduction have any connections with other boundaries in the deep Earth? The present study suggests that a mantle discontinuity near 920 km [39] may be a particularly important geodynamic barrier and may be a chemical interface. Linear undulations in the geoid show a strong peak near the 1000 km wavelength, possibly indicating a boundary near the 1000 km depth [52]. The 670 km discontinuity is large and sharp but the high seismic velocity gradient below it [53,54] suggests that the homogeneous part of the lower mantle is deeper. The lower mantle may start between the depths of 900 and 1000 km, as in its original placement by Bullen and Gutenberg. The question of whether slabs sink into the lower mantle is replaced by the question: where does the lower mantle start?

6. Conclusion

The amount of subducted plate volume during the past 130 Ma is reconstructed based on updated finite-rotation data and a digital age map of the oceanic crust. About 3.45×10^{10} km^3 of oceanic lithosphere has been subducted during the past 130 Ma, with maximum accumulation beneath Southeast Eurasia. Excellent correlations are found at harmonic degree 2 between subduction and seismic anomaly patterns over the depth range of about 800–1100 km. The regions with large amounts of subduction correlate with high velocity anomalies, in terms of both location and relative amplitude. The depth range of most robust correlation is near a probable seismic discontinuity. The correlation may indicate that (a) slabs accumulate at mid-mantle depths (mesosphere), (b) the boundary between the upper and lower mantle is closer to 920 km rather than to 670 km, (c) lower mantle downwellings control where subduction takes place, or (d) pre-existing cold regions of the mantle control the locations of post-Pangea subduction zones.

If there is a chemical boundary near 900 km it should have very large relief in a convecting mantle, much higher than phase boundaries with reasonable Clapeyron slopes. This may explain why it is relatively difficult to detect by conventional (stacking) seismology. If this is an important geodynamic boundary, as we suggest, we can refer to the 400 km to about 900 km depth range as the mesosphere, to distinguish it from the transition region and lower mantle.

Acknowledgements

We gratefully acknowledge assistance from Shingo Watada, Dietmar Müller, Lisa Gahagan and Joann Stock, and critical reviews by Michael Gurnis, David Yuen and an anonymous reviewer. We also thank Jean-Yves Royer, Mike Coffin, Lisa Gahagan and the UT Austin Plates Project for plate reconstruction maps and the UCSD group for the tomographic models. This work was funded by NSF grant EAR 92-18390 and is contribution 5455 of the Division of Geological and Planetary Sciences, California Institute of Technology. [*RV*] [38]

References

[1] B. Isacks and P. Molnar, Distribution of stresses in the descending lithosphere from a global survey of focal mechanism solutions of mantle earthquakes, Rev. Geophys. Space Phys. 9, 103–174, 1971.

[2] H.-W. Zhou and D.L. Anderson, Search for deep slabs in the northwest Pacific mantle, Proc. Natl. Acad. Sci. USA 86, 8602–8606, 1989.

[3] P.M. Shearer and G. Masters, Global mapping of topography on the 660-km discontinuity, Nature 355, 791–796, 1992.

[4] T.H. Jordon and W.S. Lynn, A velocity anomaly in the lower mantle, J. Geophys Res. 79, 2679–2685, 1974.

[5] K.C. Creager and T.H. Jordon, Slab penetration into the lower mantle beneath the Mariana and other island arcs of the Northwest Pacific, J. Geophys. Res. 91, 3573–3589, 1988.

[6] J.E. Vidale and D. Garcia-Gonzalez, Seismic observation of a deep slab, Geophys. Res. Lett. 15, 369–372, 1988.

[7] H.-W. Zhou, D.L. Anderson and R.W. Clayton, Modeling of residual spheres for subduction zone earthquakes 1. Apparent slab penetration signatures in the NW Pacific caused by deep diffused mantle anomalies, J. Geophys. Res. 95, 6799–6827, 1990.

[8] H.-W. Zhou and R.W. Clayton, P and S Wave travel time inversions for subducting slab under the island arcs of Northeast Pacific, J. Geophys. Res. 95, 6829–6851, 1990.

[9] Y. Fukao, S. Maruyama, M. Obayashi and H. Inoue, Geologic implication of the whole mantle P-wave tomography, J. Geol. Soc. Jpn 100, 4–23, 1994.

[10] R. van der Hilst, R. Engdahl, W. Spakman and G. Nolet, Tomographic imaging of subducted lithosphere below northwest Pacific island arcs, Nature 353, 37–43, 1991.

[11] U.R. Christensen and D.A. Yuen, The interaction of a subducting lithospheric slab with a chemical or phase boundary, J. Geophys. Res. 89, 4389–4402, 1984.
[12] U.R. Christensen and D.A. Yuen, Layered convection induced by phase transitions, J. Geophys. Res. 90, 10291–10300, 1985.
[13] P. Machetel and P. Weber, Intermittent layered convection in a model mantle with an endothermic phase change at 670 km, Nature 350, 55–57, 1991.
[14] P.J. Tackley, D.J. Stevenson, G.A. Glatzmaier and G. Schubert, Effects of an endothermic phase transition at 670 km depth in a spherical model of convection in the Earth's mantle, Nature 361, 699–704, 1993.
[15] S. Zhong and M. Gurnis, Mantle convection with plates and mobile, faulted plate margins, Science, submitted, 1994.
[16] S. Honda, S. Balachander, D. Yuen and D. Reuteler, Three-dimensional mantle dynamics with an endothermic phase transition, Science 259, 1308–1311, 1993.
[17] C. Scrivner and D.L. Anderson, The effect of post-Pangea subduction of global mantle tomography and convection, Geophys. Res. Lett. 19, 1053–1056, 1992.
[18] C.R. Scotese, ed., Atlas of Phanerozoic Plate Tectonic Reconstructions, International Lithosphere Program, PALEOMAP Project, 1990.
[19] D.C. Engebretson, K.D. Kelley, H.J. Cashman and M.A. Richards, 180 million years of subduction, Geol. Soc. Am. Today, pp. 93–100, 1992.
[20] M.A. Richards and D.C. Engebretson, Large-scale mantle convection and the history of subduction, Nature 335, 437–440, 1992.
[21] O. Cadek, D.A. Yuen, V. Steinbach, A. Chopelas and C. Matyska, Lower mantle thermal structure deduced from seismic tomography, mineral physics and numerical modelling, Earth Planet. Sci. Lett. 121, 385–402, 1994.
[22] D.L. Turcotte and G. Schubert, Geodynamics: Application of Continuum Physics to Geological Problems, Wiley, New York, 1992.
[23] J.-Y. Royer, R.D. Müller, L.M. Gahagan, L.A. Lawver, C.L. Mayers, D. Nurnberg and J.G. Sclater, A global isochron chart, Univ. Texas Inst. Geophys. Tech. Rep. 117, 38 pp., 1992.
[24] R.D. Müller, J.-Y. Royer and L.A. Lawver, Revised plate motions relative to the hotspots from combined Atlantic and Indian Ocean hotspot tracks, Geology 21, 275–278, 1993.
[25] R.D. Müller, W.R. Roest, J.-Y. Royer, L.M. Gahagan and J.G. Sclater, A digital age map of the ocean floor. SID Ref. Ser. 93–30, 1993.
[26] X. LePichon and J.-M. Gaulier, The rotation of Arabia and the Levant fault system, Tectonophysics 153, 271–294, 1988.
[27] S.P. Srivastava and W.R. Roest, Seafloor spreading history II–IV, in: East Coast Basin Atlas Series: Labrador Sea, J. Bell, Coord., Atl. Geosci. Cent., Geol. Surv. Can., Map Sheets L17-2–L17-6, 1989.
[28] L.A. Lawver, R.D. Müller, S.P. Srivastava and W. Roest, The Opening of the Arctic Ocean, in: Geologic History of the Polar Oceans: Arctic Versus Antarctic (NATO Symp., Oct. 1988, Bremen, Germany), U. Bleil and J. Thieds, eds., pp. 29–62, 1990.
[29] C.L. Mayers, L.A. Lawver and D.T. Sandwell, Tectonic history and new isochron chart of the South Pacific, J. Geophys. Res. 95, 8543–8567, 1990.
[30] J. Stock and P. Molnar, Revised history of early Tertiary plate motion in the south-west Pacific, Nature 325, 495–499, 1987.
[31] L.A. Lawver and C.R. Scotese, A revised reconstruction of Gondwanaland, in: Gondwana Six: Structure, Tectonics, and Geophysics, G.D. McKenzie, ed., Am. Geophys. Union Geophys. Monogr. 40, 17–24, 1987.
[32] D.C. Engebretson, A. Cox and R. Gordon, Relative motions between oceanic plates of the Pacific basin, J. Geophys. Res. 89, 10291–10310, 1984.
[33] D.C. Engebretson, A. Cox and R. Gordon, Relative motions between oceanic and continental plates in the Pacific basin, Geol. Soc. Am. Spec. Pap. 206, 59 pp., 1985.
[34] T. Tanimoto, Long-wavelength S-wave velocity structure throughout the mantle, Geophys. J. Int. 100, 327–336, 1990.
[35] W.-J. Su, R.L. Woodward and A.M. Dziewonski, Degree 12 model of shear velocity heterogeneity in the mantle, J. Geophys. Res. 99, 6945–6980, 1994.
[36] G. Master, H. Bolton and P. Shearer, Large-scale 3-dimensional structure of the mantle, Eos. Trans. Am. Geophys. Union 73(14), 201, 1992 (Spring Meet. Suppl.).
[37] H. Inoue, Y. Fukao, K. Tanabe and Y. Ogata, Whole mantle P-wave travel time tomography, Phys. Earth Planet. Inter. 59, 294–328, 1990.
[38] W.-J. Su and A.M. Dziewonski, Predominance of long-wavelength heterogeneity in the mantle, Nature 352, 121–126, 1991.
[39] H. Kawakatsu and F. Niu, Seismic evidence for a 920-km discontinuity in the mantle, Nature 371, 301–305, 1994.
[40] T.W. Ray and D.L. Anderson, Spherical disharmonics in the earth sciences and spatial solution: Ridges, hotspots, slabs, geochemistry and tomography correlations, J. Geophys. Res. 99, 9605–9614, 1994.
[41] Z. Garfunkel, Growth, shrinking and long-term evolution of plates and their implications for the tectonics of the overriding plate, J. Geophys. Res. 80, 4425–4432, 1975.
[42] Z. Garfunkel, C.A. Anderson and C. Schubert, Mantle circulation and the lateral migration of subducted slabs, J. Geophys. Res. 91, 7205–7223, 1986.
[43] D.L. Anderson, Superplumes or supercontinents?, Geology 22, 39–42, 1994.
[44] D.L. Anderson, Theory of the Earth, Blackwell, Boston, 1989.
[45] D.L. Anderson, Thermally induced phase changes, lateral heterogeneity of the mantle, continental roots and deep slab anomalies, J. Geophys. Res. 92, 13968–13980, 1987.
[46] D.L. Anderson, The upper mantle transition region: Eclogite?, Geophys. Res. Lett. 6, 433–436, 1979.
[47] S.E. Kesson, J.D. Fitz Gerald and J.M.G. Shelley, Mineral chemistry and density of subducted basaltic crust at lower mantle pressures, Nature 372, 767–769, 1994.

[48] S. Kirby, W. Durhan and L. Stern, Mantle phase changes and deep earthquake faulting in subducting lithosphere, Science 252, 216–225, 1991.
[49] D.L. Anderson and J.D. Bass, Mineralogy and composition of the upper mantle, Geophys. Res. Lett. 11, 637–640, 1984.
[50] D.L. Anderson, Chemical stratification of the mantle, J. Geophys. Res. 84, 6297–6298, 1979.
[51] R. van der Hilst and T. Seno, Effects of relative plate motion on the deep structure and penetration depth of slabs below the Izu–Bonin and Mariana island arcs, Earth Planet. Sci. Lett. 120, 395–407, 1993.
[52] P. Wessel, D. Bercovici and L. Kroenke, The possible reflection of mantle discontinuities in the Pacific geoid and bathymetry, Geophys. Res. Lett. 21, 1943–1946, 1994.
[53] A. Dziewonski and D.L. Anderson, Preliminary reference Earth model, Phys. Earth Planet. Inter. 25, 297–356, 1981.
[54] S. Grand and D.V. Helmberger, Upper mantle shear structure of North America, Geophys., J.R. Astron. Soc. 76, 339–438, 1984.